Field emission efficiency of a carbon nanotube array under parasitic nonlinearities

Anand, S.V., Mahapatra, D.R., Sinha, N.,
Yeow, J.T.W., Melnik, R.V.N.

Proceedings of the
ASME International Mechanical Engineering Congress and Exposition (IMECE2010, Nov., Vancouver, Canada,
Paper: IMECE2010-39558, 10 pages),
ASME, Vol. 10, pp. 609 - 618, 2012.

Proceedings of the ASME 2010 International Mechanical Engineering Congress & Exposition
IMECE2010
November 12-18, 2010, Vancouver, British Columbia, Canada

IMECE2010-39558

FIELD EMISSION EFFICIENCY OF A CARBON NANOTUBE ARRAY UNDER PARASITIC NONLINEARITIES

Sandeep V. Anand
Department of Aerospace Engineering,
Indian Institute of Science,
Bangalore 560012, India

D. Roy Mahapatra
Department of Aerospace Engineering, Indian Institute of Science
Bangalore 560012, India

Niraj Sinha
Department of Mechanical Engineering, Massachusetts Institute of Technology,
Cambridge, MA 02139, USA

J.T.W. Yeow
Department of Systems Design Engineering, University of Waterloo, Waterloo, ON,
N2L 3G1, Canada

R.V.N. Melnik
M^{2}NeT Lab, Wilfrid Laurier University, Waterloo, ON,
N2L3C5, Canada and BCAM,
Bizkaia Technology Park, 48160
Derio, Spain

ABSTRACT

Carbon Nanotubes (CNTs) grown on substrates are potential electron sources in field emission applications. Several studies have reported the use of CNTs in field emission devices, including field emission displays, X-ray tube, electron microscopes, cathode-ray lamps, etc. Also, in recent years, conventional cold field emission cathodes have been realized in micro-fabricated arrays for medical X-ray imaging. CNT-based field emission cathode devices have potential applications in a variety of industrial and medical applications, including cancer treatment. Field emission performance of a single isolated CNT is found to be remarkable, but the situation becomes complex when an array of CNTs is used. At the same time, use of arrays of CNTs is practical and economical. Indeed, such arrays on cathode substrates can be grown easily and their collective dynamics can be utilized in a statistical sense such that the average emission intensity is high enough and the collective dynamics lead to longer emission life. The authors in their previous publications had proposed a novel approach to obtain stabilized field emission current from a stacked CNT array of pointed height distribution. A mesoscopic modeling technique was employed, which took into account electro-mechanical forces in the CNTs, as well as transport of conduction electron coupled with electron–phonon induced heat generation from the CNT tips. The reported analysis of pointed arrangements of the array showed that the current density distribution was greatly localized in the middle of the array, the scatter due to electrodynamic force field was minimized, and the temperature transients were much smaller compared to those in an array with random height distribution.

In the present paper we develop a method to compute the emission efficiency of the CNT array in terms of the amount of electrons hitting the anode surface using trajectory calculations. Effects of secondary electron emission and parasitic capacitive nonlinearity on the current-voltage signals are accounted. Field emission efficiency of a stacked CNT array with various pointed height distributions are compared to that of arrays with random and uniform height distributions. Effect of this parasitic nonlinearity on the emission switch-on voltage is estimated by model based simulation and Monte Carlo method.

INTRODUCTION

Field emission from carbon nanotubes (CNTs) was first reported in 1995 by three research groups (1, 2 and 3). With significant research attention, CNTs are currently ranked among the best field emitters. CNTs grown on substrates are used as electron sources in field emission applications. Several studies have reported the use of CNTs in field emission

devices, including field emission displays, X-ray tube sources, electron microscopes, cathode-ray lamps, etc. (4, 5, 6 and 7). Also, in recent years, conventional cold field emission cathodes have been realized in micro-fabricated arrays for medical X-ray imaging (8) and today CNT-based field emission cathode devices can readily produce both continuous and pulsed X-ray for a variety of industrial and medical applications (9), including recent applications for cancer treatment (10). Field emission performance of a single isolated CNT is found to be remarkable, but the situation becomes complex when an array of CNTs is used (11). At the same time, use of arrays of CNTs is known to be practical and economical. Indeed, such arrays on cathode substrates can be grown easily and their collective dynamics can be utilized in a statistical sense such that the average emission intensity is high enough and the collective dynamics lead to longer emission life. The modeling process of CNT arrays and associated devices requires the development of multiphysics approaches due to a range of coupled processes and transport phenomena involved (12, 13). This development has been discussed in detail in recent papers (14, 15, 16, 17, 31, 32). In particular, in Ref. (14) field emission properties of open and closed single-walled CNTs were analyzed. In (15), for the first time a systematic multiphysics based modeling approach was proposed to analyze the evolution and self-assembly of randomly oriented CNTs and the results of this analysis were applied to thin-film emitting diodes. Electromechanical effects in such devices were studied in detail in Ref. (16) as these effects are known to be able to augment significantly the properties of nanostructures (18). More recently, in Ref. (17) a systematically coupled model accounting for both the electron–phonon transport and the mechanical deformation in the CNTs has been proposed. Based on earlier analyses, we have concluded that field emission from CNTs is difficult to characterize using simple formulae or data fitting due to several physical phenomena involved: (1) electron–phonon interaction; (2) electro-mechanical force field leading to deformation of CNTs; and (3) ballistic transport induced thermal spikes, coupled with high dynamic stress, leading to degradation of emission performance. Recently, a number of advances have been made along these lines. Indeed, fairly detailed physics-based models of CNTs considering the aspects (1) and (2) above have already been developed by the authors (17, 19 and 20). For a matrix of CNTs, an analytical estimate of field enhancement factor including the effect of Coulomb field, image potential and anode–cathode distance was reported by Wang et al. (21). Effects of vertical alignment of CNTs and substrates on the field emission current–voltage characteristics were studied experimentally by Chen et al. (22). Effect of spacing and diameter of CNTs in the arrays have been studied in Ref. (23). Advances in patterning of CNTs for field emission applications have also been recently made (see e.g. Ref. (24)).

In Ref. (15), the present authors developed a model of interacting CNTs including the effect of random CNTs on cathode substrate (termed as a CNT based thin film). The I–V curves obtained from this model were compared with experimental results and found to be in good agreement. Subsequent analysis of the transient phenomena and statistics of the CNT arrays were analyzed both experimentally and based on a refined version of the previous model of CNT array in Refs. (16, 17). With reference to this model, one would be able to realize how the present idea of pointed array of CNTs has been developed. However, design optimization issues aimed at better field emission devices to reduce the extent of electro-mechanical fatigues and to improve spatio-temporal localization of emitted electrons remain open and are important areas of research. With due success in designing such devices, various applications such as in situ biomedical X-ray probes and thin film pixel based imaging technology, to name just a few, are of great significance. The concept of high resolution surface imaging using a pointed array was CNTs was explored in Ref. (30). The authors' interest towards this study stems from the problem of precision biomedical X-ray generation. In this paper, we focus on the device-level performance of CNTs grown on a metallic surface in the form of an array (for field emission) under diode configuration. We analyze a new design concept, wherein (a) the electrodynamic force field leading to strong electron–phonon interaction during ballistic transport and also (b) the usually observed reorientation of the CNT tips and instability due to Coulomb repulsions can be harnessed optimally. The emission efficiencies of the CNT arrays is evaluated in terms of the amount electrons hitting the anode surface using trajectory calculations. Effects of secondary electron emission and parasitic capacitive nonlinearity on the current-voltage signals are accounted for. Field emission efficiency of a stacked CNT array with various pointed height distributions are compared to that of arrays with random and uniform height distributions.

MODEL FORMULATION

We first discuss the basic modeling framework in this section and then formulate the model of electrodynamic force field by considering individual CNTs in the array as one-dimensional elements for transport of electron-gas with appropriate boundary conditions.

Let N_T be the total number of carbon atoms including those in CNTs and those in cluster forms as a mesoscopic description of the surface of the cathode substrate and in a representative volume element $V_{cell} = \Delta A d$. Here ΔA is the computational cell surface interfacing the anode and d is the distance between the inner surfaces of cathode substrate and the anode. Let N be the number of CNTs in the cell, and N_{CNT} be the total number of carbon atoms present in the CNTs. We assume

that during field emission, some of the CNT structures are decomposed and they form clusters. Such degradation and fragmentation of CNTs can be treated as the reverse process of CVD or a similar growth process used for producing the CNTs on a substrate. Hence,

$$N_T = NN_{CNT} + N_{cluster}\,, \tag{1}$$

where $N_{cluster}$ is the total number of carbon atoms in the clusters in a cell at time t and it is given by

$$N_{cluster} = V_{cell}\int_0^t dn_1(t)\,, \tag{2}$$

where n_1 is the concentration of carbon clusters in the cell. By combining Eqs. (1) and ((2)), one has

$$N = \frac{1}{N_{CNT}}\left[N_T - V_{cell}\int_0^t dn_1(t)\right]. \tag{3}$$

The number of carbon atoms in a CNT is proportional to its length. Let the length of a CNT be a function of time, denoted as $L(t)$. Therefore, one can write

$$N_{CNT} = N_{ring}L(t)\,, \tag{4}$$

where N_{ring} is the number of carbon atoms per unit length of a CNT and it can be determined from the geometry of the hexagonal arrangement of carbon atoms in the CNT. By combining Eqs. (3) and (4), one can write

$$N = \frac{1}{N_{ring}L(t)}\left[N_T - V_{cell}\int_0^t dn_1(t)\right]. \tag{5}$$

In order to determine $n_1(t)$ phenomenologically, we employ a nucleation coupled model developed previously in Ref. (19). Based on the model, the rate of degradation of CNTs (v_{burn}) is defined as

$$v_{burn} = V_{cell}\frac{dn_1(t)}{dt}\left[\frac{s(s-a_1)(s-a_2)(s-a_3)}{n^2a_1^2 + m^2a_2^2 + nm(a_1^2+a_2^2-a_3^2)}\right]^{1/2} \tag{6}$$

where a_1, a_2, a_3 are lattice constants, $s = \frac{1}{2}(a_1+a_2+a_3)$, n and m are integers $(n \geq |m| \geq 0)$. The pair (n,m) defines the chirality of the CNT. Therefore, at a given time, the length of a CNT can be expressed as $h(t) = h_0 - v_{\text{burn}}t$, where h_0 is the initial average height of the CNTs and d, as before, is the distance between the cathode substrate and the anode.

The surface electron density of CNTs ($\tilde{n}$) can be expressed as the sum of a steady (unstrained) part ($\tilde{n}_0$) and a dynamically strained part ($\tilde{n}_0$). Therefore, $\tilde{n} = \tilde{n}_0 + \tilde{n}_1$, where the steady part $\tilde{n}_0$ is the surface electron density corresponding to the Fermi level energy in the unstrained CNT and it can be approximated as (25) $\tilde{n}_0 = kT/(\pi b^2\Delta)$, where k is Boltzmann's constant, T is the absolute temperature, b is the interatomic distance and Δ is the overlap integral ($\approx 2eV$ for carbon). The fluctuating part $\tilde{n}_1$ is inhomogeneous along the length of the CNTs. Actually, $\tilde{n}_1$ should be coupled nonlinearly with the deformation and the electromagnetic field (26). However, in a simplified form, $\tilde{n}_1$ is primarily governed by one of the quantum-hydrodynamic equations. The deformation of CNTs during field emission is a combined effect of various electromechanical forces in a slow time scale and the fluctuation of the CNT sheet due to electron-phonon interaction in a fast time scale. Therefore, the total displacement u_{total} can be expressed as

$$u_{\text{total}} = u^{(1)} + u^{(2)}\,, \tag{6}$$

where $u^{(1)}$ and $u^{(2)}$ are the displacements due to electromechanical forces and fluctuation of CNT sheets due to electron-phonon interaction, respectively. The elements of displacement vector in the coordinate system (x', y', z') with z' being the tangent to the curved tube axis, can be written as

$$u^{(1)} = \{u_{x'}^{(1)}\ u_{z'}^{(1)}\}^T\,, \quad u^{(2)} = \{u_{x'}^{(2)}\ u_{z'}^{(2)}\}^T\,, \tag{7}$$

where $u_{x'}$ is the lateral displacement and $u_{z'}$ is the longitudinal displacement at a length-wise location of CNTs, where the CNT cross-sections are reduced to a point, thus neglecting the radial breathing modes. Furthermore, to simplify the analysis, we consider only one component of lateral motion and remove the y' dependence of the motion in the slow time scale. In the array, each CNT is treated as a one-dimensional elastic member discretized by fictitious segments and nodes with equivalent electronic charges lumped on the nodes. The electrodynamic force field is computed as discussed in Ref. (17).

In the fast time scale, the displacement field $u^{(2)}$ is coupled with the density of state via the changes in the atomic coordinates due to electrodynamic force. The electrodynamic force field comprises of Coulomb force due to pair-wise interaction of CNTs in the array and the electrodynamic force due to conduction electrons within a CNT. The density of state is further influenced by the electromagnetic field and self-interaction potentials. Such a dynamic interaction between the electrons and the electromagnetic field can be expressed as

$$\frac{\partial^2 \tilde{n}_1}{\partial t^2} - \frac{e\tilde{n}_0}{m_e}\frac{\partial E_{z'}}{\partial z'} - \alpha_2 \frac{\partial^2 \tilde{n}_1}{\partial z'^2} + \beta_2 \frac{\partial^4 \tilde{n}_1}{\partial z'^4} + \frac{\beta_2}{r^2}\frac{\partial^2}{\partial z'^2}\left(\frac{\partial^2 \tilde{n}_1}{\partial \theta_0^2}\right)$$
$$+ \frac{n_0}{m_e}\frac{\partial f_{lz'}}{\partial z'} - \frac{e\tilde{n}_0}{m_e}\frac{1}{r}\frac{\partial E_{\theta_0}}{\partial \theta_0} - \frac{\alpha_2}{r^2}\frac{\partial^2 \tilde{n}_1}{\partial \theta_0^2} + \frac{\beta_2}{r^4}\frac{\partial^4 \tilde{n}_1}{\partial \theta_0^4}$$
$$+ \frac{\beta_2}{r^2}\frac{\partial^2}{\partial \theta_0^2}\left(\frac{\partial^2 \tilde{n}_1}{\partial z'^2}\right) + \frac{n_0}{m_e}\frac{1}{r}\frac{\partial f_{l\theta_0}}{\partial \theta_0} - \frac{en_0}{m_e}\frac{\partial E_r}{\partial r}$$
$$+ \frac{n_0}{m_e}\frac{\partial f_{lr}}{\partial r} + \frac{n_0}{m_e}\frac{\partial f_{pr}}{\partial r} = 0, \quad (9)$$

where (r, θ_0, z') defines the cylindrical coordinate system for a CNT with $r = R$ as the CNT radius, m_e is the effective mass of electron, α_2 is the speed of propagation of density disturbances, β_2 is the single electron excitation in the electron gas, f_l is the Lorentz force, f_p is the ponderomotive force, and $E_{z'}$, E_{θ_0} and E_r are the axial, circumferential and out-of-plane components of the electric field, respectively. The electric field satisfies the Maxwell's equation for the effective medium:

$$\nabla^2 E - \mu\sigma\frac{\partial E}{\partial t} - \mu\varepsilon\frac{\partial^2 E}{\partial t^2} = \mu\frac{\partial J}{\partial t}, \quad (10)$$

where μ, σ, ε, and J are the magnetic permeability, electric conductivity, electric permittivity, and electric current density in a CNT as an effective medium, respectively. The current density in the CNT sheet can be approximated as

$$J \approx e\tilde{n}\left(v_0 + \frac{\partial u_{z'}^{(2)}}{\partial t} + c_p\frac{\partial u_{z'}^{(2)}}{\partial z'}\right), \quad (11)$$

where v_0 is the velocity of conduction electrons in the unstrained CNT, c_p is the phase speed of sound propagation along z' direction. Substituting this in Eq. (9) and expanding, we get

$$\frac{\partial^2 E_{z'}(r)}{\partial z'^2} + \frac{1}{r^2}\frac{\partial^2 E_{z'}(r)}{\partial \theta_0^2} + \frac{1}{r}\frac{\partial}{\partial r}\left(r\frac{\partial E_{z'}(r)}{\partial r}\right) - \mu\sigma\frac{\partial E_{z'}(r)}{\partial t}$$
$$-\mu\varepsilon\frac{\partial^2 E_{z'}(r)}{\partial t^2} = \mu\frac{\partial}{\partial t}\left(e\tilde{n}\frac{\partial u_{z'}^{(2)}}{\partial t}\right), \quad (12)$$

$$\frac{\partial^2 E_{\theta_0}(r)}{\partial z'^2} + \frac{1}{r^2}\frac{\partial^2 E_{\theta_0}(r)}{\partial \theta_0^2} + \frac{1}{r}\frac{\partial}{\partial r}\left(r\frac{\partial E_{\theta_0}(r)}{\partial r}\right)$$
$$-\mu\sigma\frac{\partial E_{\theta_0}(r)}{\partial t} - \mu\varepsilon\frac{\partial^2 E_{\theta_0}(r)}{\partial t^2} = 0, \quad (13)$$

$$\frac{\partial^2 E_r(r)}{\partial z'^2} + \frac{1}{r^2}\frac{\partial^2 E_r(r)}{\partial \theta_0^2} + \frac{1}{r}\frac{\partial}{\partial r}\left(r\frac{\partial E_r(r)}{\partial r}\right)$$
$$-\mu\sigma\frac{\partial E_r(r)}{\partial t} - \mu\varepsilon\frac{\partial^2 E_r(r)}{\partial t^2} = 0. \quad (14)$$

In the absence of electronic transport within and field emission from the tip of a CNT, the background electric field is simply $E_0 = -V_0/d$, where $V_0 = V_d - V_s$ is the applied bias voltage, V_s is the constant source potential on the substrate side, V_d is the drain potential on the anode side and d, as before, is the clearance between the electrodes. The total electrostatic energy consists of a linear drop due to the uniform background electric field and the potential energy due to the charges on the CNTs. Therefore, the total electrostatic energy can be expressed as

$$\mathrm{V}(x,z) = -eV_s - e(V_d - V_s)\frac{z}{d} + \sum_j G(i,j)(\hat{n}_j - n), \quad (15)$$

where e is the positive electronic charge, $G(i,j)$ is the Green's function (27) with i indicating the ring position and $\hat{n}_j$ describing the electron density at node position j on the ring. In the present case, while computing the Green's function, we also consider the nodal charges of the neighboring CNTs. This essentially introduces non-local contributions due to the array of CNTs. We compute the total electric field $\mathbf{E} = -\nabla \mathrm{V}/e$, which is expressed as

$$E_z = -\frac{1}{e}\frac{d\mathrm{V}(z)}{dz}. \quad (16)$$

The current density (J) due to field emission is obtained by using the Fowler-Nordheim equation Ref. (28)

$$J = \frac{BE_z^2}{\Phi}\exp\left[-\frac{C\Phi^{3/2}}{E_z}\right], \quad (17)$$

where Φ is the work function of the CNT, and B and C are constants. Computation is performed at every time step, followed by update of the geometry of the CNTs. As a result, the charge distribution among the CNTs also changes and such a change affects the electrostatic energy according to Eq. (14). The field emission current (I_{cell}) from the anode surface corresponding to an elemental volume V_{cell} containing an array of CNTs is then obtained as

$$I_{\text{cell}} = A_{\text{cell}}\sum_{j=1}^{N} J_j, \quad (18)$$

where A_{cell} is the anode surface area and N is the number of CNTs in the volume element. The total current is obtained by summing the cell-wise current (I_{cell}). This formulation takes

into account the effect of CNT tip orientations, and one can perform statistical analysis of the device current for randomly distributed and randomly oriented CNTs.

Parasitic Non-linearities

The above equations are valid as long as we assume that the field emission current is purely due to the emission of primary electrons from the cathode substrate toward the anode substrate. At low DC voltages such an assumption is valid because the applied voltage is only sufficient to extract the electrons from the metallic cathode substrate and accelerate them towards the anode surface. But at high voltages and at high frequency AC voltages such an assumption may not hold as many other non-linear parasitic phenomena also occur which may alter the field emission current. For the sake of simplicity, we limit the scope of our analysis to only two such phenomena, namely (1) secondary electron emission from the anode due to high kinetic energy of the emitted primary electrons and (2) application of high frequency AC electric field across the cathode and anode.

We first compute the kinetic energy of the primary electrons hitting the surface of the anode E_{in}. The force F experience by an electron coming out of the cathode substrate may be written as $F = eE_Z$ where E_Z is the applied electric field and e is the charge on an electron. Therefore, the acceleration A of the electron in the space between the cathode and anode may be written as A = Force/Electron mass = eE_Z / m_e, where m_e is the mass of a single electron. The kinetic energy of the primary electron which is about to strike the anode may be written as $\mathrm{E}_{in} = \frac{1}{2} m_e v_{final}^2$, where v_{final} is the velocity of the primary electron at the time of impact with the anode and may be written as $v_{final} = \sqrt{2eE_Z h / m_e}$. Thus, E_{in} becomes

$$\mathrm{E}_{in} = \frac{1}{2} m_e n_p \left[\frac{2eE_Z h}{m_e} \right]. \quad (19)$$

Next we write the energy equations for the two electrodes in terms of the applied electric field and the work functions of the electrode materials. The cathode equation for energy exchange can be written as E_{in} = applied electrical energy – work function or

$$\frac{1}{2} m_e n_p \left[\frac{2eE_Z h}{m_e} \right] = \left(n_p - n_s \right) e\left(-V\right) - n_p \left(\Phi_{cathode} - E_{Fcathode} \right), \quad (20)$$

where $E_{Fcathode}$ is the Fermi energy of the cathode material. n_p and n_s are the number of emitted primary and secondary electrons, respectively. Eq. 20 gives us the value of n_s. Similarly, the anode equation for energy exchange may be written as

$$\mathrm{E}_{in} = \left[\Phi_{Anode} + \left(n_s + n_p \right) e\left(-V\right) - E_{FAnode} \right] + \mathrm{E}_{out} + \text{Damping}. \quad (21)$$

where E_{out} is the kinetic energy of the emitted secondary electrons from the anode surface and E_F is the Fermi energy. The damping term is included in Eq. 21 because the secondary electrons have to travel against the direction of the applied electric field and hence their kinetic energy gradually decreases, while traveling from the anode surface to the cathode surface.

Eq. (21) may be expanded as

$$\frac{1}{2} m_e n_p \left[\frac{2eE_Z h}{m_e} \right] = \mathrm{E}_{out} + \left[2\left(\frac{-eE_Z}{m_e} \right) h \right] + \left[\Phi_{Anode} + \left(n_p + n_s \right) e\left(-V\right) - E_{FAnode} \right]. \quad (22)$$

After having computed E_{out} from Eq. (22) we move on to compute the new field emission current density.

In order to compute the modified current density considering the effect of secondary electron emission from the anode substrate we re-write the Fowler-Nordheim equation (Eq. 17) as

$$J = \left(\dot{n}_p - \dot{n}_s \right) e = \frac{B E_Z^2 \exp\left[-C\left(\Phi - E_F + n_s e\left(-V\right) \right)^{3/2} E_Z \right]}{\left(\Phi_{cathode} - E_F \right) + n_s e\left(-V\right) + \mathrm{E}_{out}}. \quad (23)$$

In Eq. (23), E_{out} is substituted from Eq. (22) and n_s is substituted from Eq. 20.

Next we compute the current density under an applied AC field of the form given in Eq. (24).

$$E_Z \approx -\frac{V_0}{h} \mathrm{Sin}\omega t. \quad (24)$$

Substituting Eq. (24) in Eq. (17) we get

$$J\left(t\right) = \frac{B V^2 \mathrm{Sin}^2 \omega t}{\phi h^2} \exp\left[C\phi^{3/2} \frac{h}{V_0 \mathrm{Sin}\omega t} \right]. \quad (25)$$

The first derivative of the current density with respect to V_0 is given as

$$\frac{dJ}{dV_0}=\frac{dJ}{d\left(V_0\mathrm{Sin}\omega t\right)}=\frac{1}{V_0}\frac{dJ}{dt}\frac{dt}{d\left(\mathrm{Sin}\omega t\right)}$$
$$=\frac{1}{V_0}\frac{dJ}{dt}\frac{1}{\omega\mathrm{Cos}\omega t}. \quad (26)$$

The time derivative of the current density is then calculated as Eq. (27):

$$\frac{dJ}{dt}=J\left(2\omega\frac{\mathrm{Cos}\omega t}{\mathrm{Sin}\omega t}\right)-J\left(\frac{1}{V_0}\phi^{3/2}Ch\frac{\omega\mathrm{Cos}\omega t}{\mathrm{Sin}^2\omega t}\right)$$
$$=\omega\frac{\mathrm{Cos}\omega t}{\mathrm{Sin}\omega t}\left[2-\frac{\phi^{3/2}C}{\left(V_0/h\right)\mathrm{Sin}\omega t}\right]J=f\left(\omega t\right)J. \quad (27)$$

Next, we find the first derivative of the current density with respect to V and is given by Eq. (28)

$$\frac{dJ}{dv}=\frac{1}{V_0}\frac{1}{\omega\mathrm{Cos}\omega t}\frac{dJ}{dt}=\frac{1}{V_0}\frac{1}{\omega\mathrm{Cos}\omega t}f\left(\omega\right)J$$
$$=\frac{1}{V_0}\frac{1}{\mathrm{Sin}\omega t}\left[2-\frac{\Phi^{3/2}C}{\left(V_0/h\right)\mathrm{Sin}\omega t}\right]J. \quad (28)$$

For static case Eq. (28) may be reduced to

$$\left(\frac{dJ}{dV}\right)_s=\frac{1}{V_0}\left[2-\frac{\Phi^{3/2}C}{\left(V_0/h\right)}\right]J_s. \quad (29)$$

Eq. (28) divided by Eq. (29) gives

$$\frac{\left(\frac{dJ}{dV}\right)}{\left(\frac{dJ}{dV}\right)_s}=\frac{1}{\mathrm{Sin}\omega t}\frac{\left[2-\frac{\Phi^{3/2}C}{\left(V_0/h\right)\mathrm{Sin}\omega t}\right]}{\left[2-\frac{\Phi^{3/2}C}{\left(V_0/h\right)}\right]}\frac{J}{J_s}. \quad (30)$$

Eq. (30) on simplification gives

$$\frac{\left(\frac{dJ}{dV}\right)}{\left(\frac{dJ}{dV}\right)_s}=\frac{\left[2-\frac{\Phi^{3/2}C}{\left(V_0/h\right)\mathrm{Sin}\omega t}\right]}{\left[2-\frac{\Phi^{3/2}C}{\left(V_0/h\right)}\right]}\mathrm{Sin}\omega t$$
$$\times\exp\left[C\Phi^{3/2}\frac{h}{V_0}\left(\frac{1}{\mathrm{Sin}\omega t}-1\right)\right]. \quad (31)$$

Then the condition for gain amplification may be written as $\left(\frac{dJ}{dV}\right)/\left(\frac{dJ}{dV}\right)_s>1$ and the condition for intensity magnification is written as $J/J_s>1$ and is given by Eq. (32)

$$C\Phi^{3/2}\frac{h}{V_0}\left(\frac{1}{\mathrm{Sin}\omega t}-1\right)>\ln\left[\frac{1}{\mathrm{Sin}^2\omega t}\right]. \quad (32)$$

RESULTS AND DISCUSSIONS

In the proposed design of CNT array based field emission, we introduce two additional gates on the edges of the cathode substrate. An array of stacked CNTs is considered on the cathode substrate. Fig. 1 shows a three-dimensional schematic of the CNT array with electrodes as a single pixel. Due to circular symmetry, we consider a two-dimensional configuration of a line of CNT array in the simulation. The height of the CNTs is such that a symmetric force field is maintained in each pixel with respect to the central axis parallel to z-axis (see Fig. 2). As a result, it is expected that a maximum current density and a well-shaped beam can be produced under DC voltage across the cathode and anode. In the present design, the anode is assumed to be simply a uniform conducting slab. However, such an anode can be replaced with a porous thin film along with MEMS-based beam control mechanism. Fig. 2 shows the transverse electric field distribution (E_z) in the pixel, which directly influences the field emission.

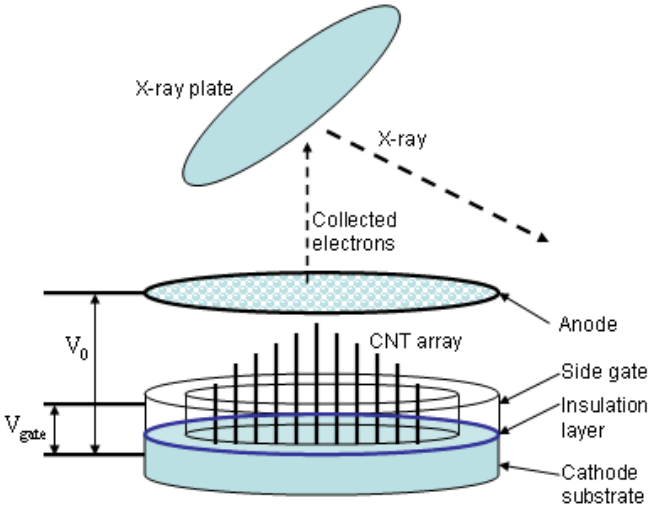

Figure 1: Schematic setup of the CNT array based field emission pixel.

We consider 100 CNTs in an array for all the simulations. In the simulations, the distance between the cathode substrate and the anode surface was taken as 34.7 μm. The height of the side-wise gates was 6 μm, while the spacing between neighboring CNTs in the array was selected as 2 μm.

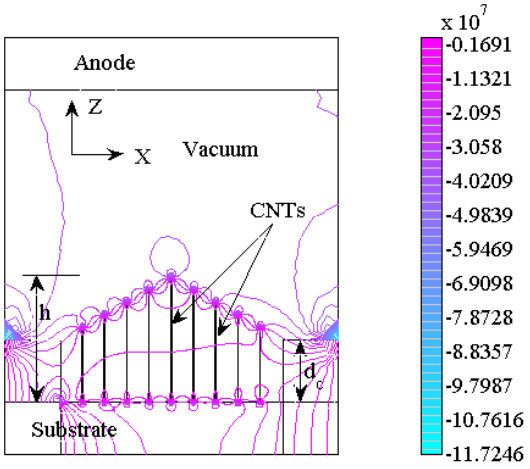

Figure 2: Contour plot showing concentration of electric field E_z surrounding the CNT tips under symmetric lateral force field. V_0=650V and the side-wise gates are shorted with the cathode substrate. Electric field contours are shown in V/m unit in the color bar.

A DC bias voltage of 650V is applied across the cathode and anode.

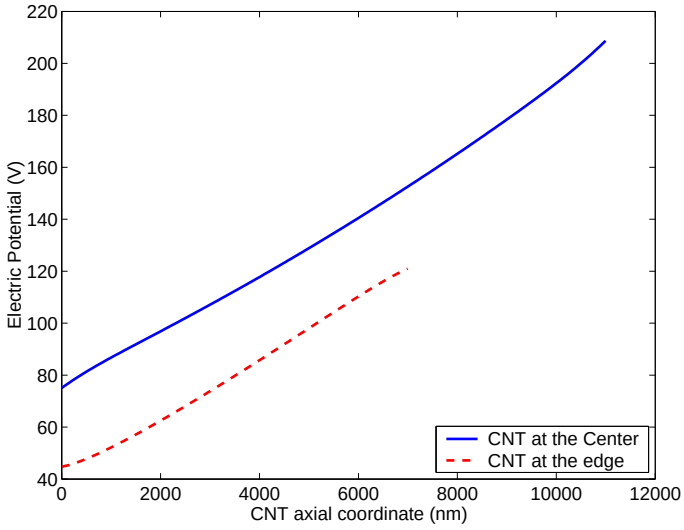

Figure 3: Distribution of electric potential along the CNTs.

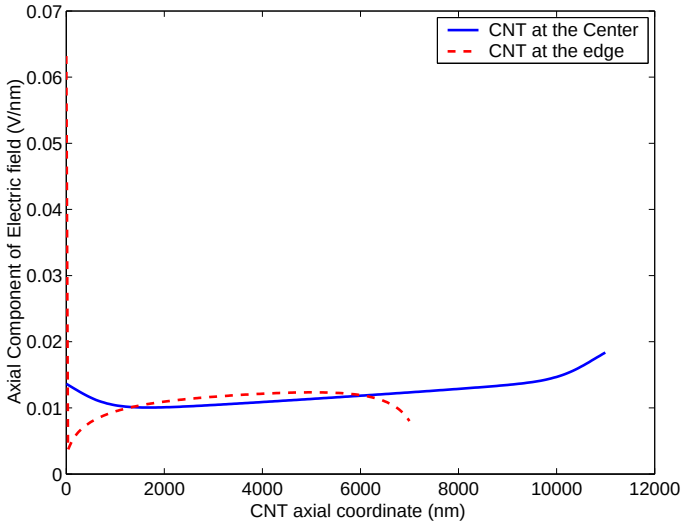

Figure 4: Distribution of transverse electric field Ez along the CNTs.

We compare the two cases of height distributions of CNTs in the array. In one of these cases, where the CNTs were stacked like a pointed shape, the height was varied from 6 μ m at the edges to 12 μ m at the centre. In the other case, we chose a random height distribution for the CNTs in the array, where the height was varied as $h = (h_0 \pm 2\mu m) \mp 2\mu m \times \text{rand}(1)$. Here, the function rand denotes random number generator. The constants B and C in Eq. (17) were taken as $\left(1.4\times10^{-6}\right)\times\exp\left(\left(9.8929\right)\times\Phi^{-1/2}\right)$ and 6.5×10^{7}, respectively (29). It has been reported in literature (e.g., Ref. (29)) that the work function F for CNTs is smaller than the work functions for metal, silicon, and graphite. However, there are significant variations in the experimental values of F depending on the types of CNTs (i.e. SWNT/MWNT) and geometric parameters. The type of substrate material also has significant influence on the electronic band-edge potential.

Fig. 3 shows the distribution of electric potential along the CNTs. Clearly, the longer CNTs at the middle is subjected to more than twice the potential at the tip of CNTs at the edge. Fig. 4 shows that the CNT tip at the middle of the array experiences only a slight increase in the electric field and hence a insignificant increase in the electrodynamic pull toward the anode. With this arrangement, it is now possible to tune the spatio-temporal quality of the emitted electron beam.

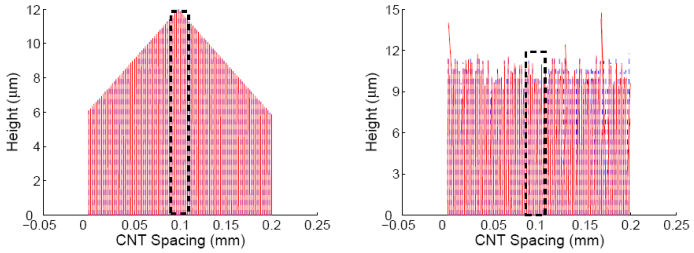

(a) (b)

Figure 5: Visualization of initial and deflected shapes of an array of 100 CNTs at t = 50s of field emission for (a) pointed and (b) random configurations. The dotted lines indicate initial CNTs.

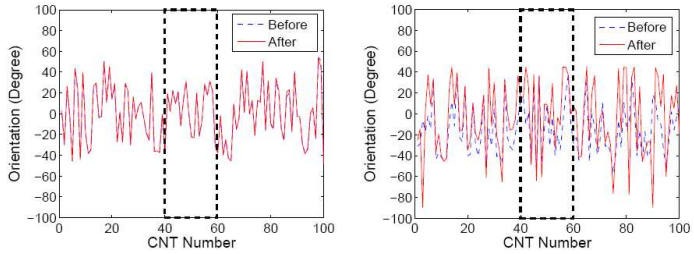

(a) (b)

Figure 6: Tip deflections of each CNT in an array of 100 CNTs at t = 50s of field emission for (a) pointed and (b) random configurations. Dotted line indicates initial tip orientation angle.

Fig. 5(a) shows well stabilized CNTs owing to the electrodynamic interaction due to the pointed shape as compared to the random distribution in Fig. 5(b). During 50 s of field emission simulated in these results, the strong influence of lateral force field can be clearly seen. Such force field produces electrodynamic repulsion such that the resultant force imbalance on the CNTs towards the edges of the array eventually destabilizes the orientation of the CNT tips. Since, in the pointed shape (see Fig. 5(a)), this force imbalance is minimized due to a gradual reduction in the CNT heights, a lesser magnitude of deflections is observed. Also, the lateral electrodynamic forces produce instabilities in the randomly distributed array, where the electrons are pulled up by the anode and the CNTs tips experience a significant elongation as shown in Fig. 5(b). This is further quantified by the tip angle distribution before and after 50 s of field emission as shown in Fig. 6(b) for a random height distribution as compared to Fig. 6(a) for the pointed shape. It should be noted that in the simulation, the initial tip deflections are prescribed as a random distribution for both the cases. Due to this reason, the tip orientation angles in Fig. 6(a) are also large in the case of pointed shape, but these do not change over time.

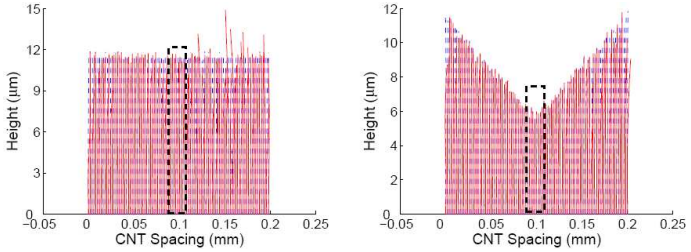

(a) (b)

Figure 7: Visualization of initial and deflected shapes of an array of 100 CNTs at t= 50s of field emission for (a) uniform height distribution (left) and (b) V-shape (right). The dotted lines indicate initial orientation of the CNTs.

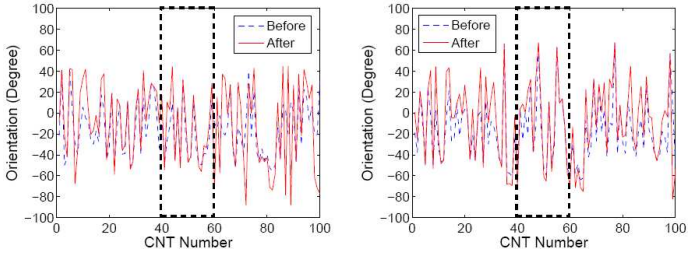

(a) (b)

Figure 8: Tip deflections of each CNT in an array of 100 CNTs at t= 50s of field emission for (a) uniform height distribution (left) and (b) V-shape (right). The dotted line indicates initial tip orientation angle.

In Figs. 7 and 8, it is shown that uniform height distribution experiences similar instability as in the case of random height distribution, whereas the V-shaped array experiences instabilities near the edges which is a moderate performance among all the four array configurations considered.

Next we simulate and compare field emission current histories for different array types under AC voltage of 650V with frequency of 10Hz (see Fig. 9). As evident from Fig. 9, the CNT array with pointed shape gives most stable current output among all the configurations considered.

Finally, we compute the field emission efficiencies for the various CNT-array configurations discussed above in terms of the amount electrons hitting the anode surface using trajectory calculations. From Fig. 10 it is clear that the pointed height distribution of the CNTs is the most efficient configuration as the calculated emission efficiency is the highest at 78.2% for a pointed height distribution with a slope of 5^0.

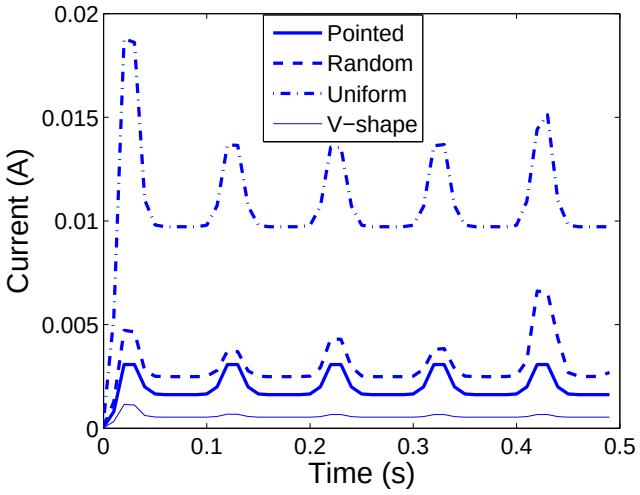

Figure 9: Comparison of field emission current histories for different array types under AC voltage of 650V with frequency of 10 Hz.

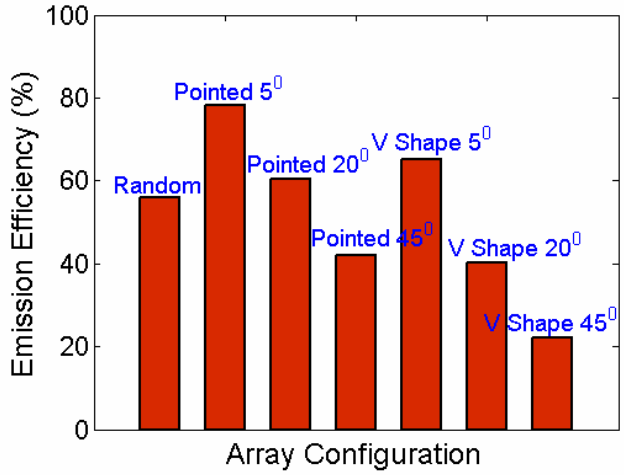

Figure 10: Field emission efficiencies for the various array configurations. For the pointed and V-shape arrays, the slope of the arrays is varied and slopes of 5^0, 20^0 and 45^0 are considered.

REFERENCES

(1) A.G. Rinzler, J.H. Hafner, P. Nikolaev, L. Lou, S.G. Kim, D. Tomanek, D. Colbert, and R.E. Smalley, Unraveling nanotubes: field emission from an atomic wire, Science 269 (1995), pp. 1550–1553.

(2) W.A. de Heer, A. Chatelain, and D. Ugrate, A carbon nano-tube field-emission electron source, Science 270 (1995), pp. 1179–1180.

(3) L.A. Chernozatonskii, Y.V. Gulyaev, Z.Y. Kosakovskaya, N.I. Sinitsyn, G.V. Torgashov, Y.F. Zakharchenko, E.A. Fedorov, and V.P. Valchuk, Electron field emission from nanofilament carbon films, Chem. Phys. Lett. 233 (1995), pp. 63–68.

(4) J.M. Bonard, J.P. Salvetat, T. Stockli, L. Forro, and A. Chatelain, Field emission from carbon nanotubes: perspectives for applications and clues to the emission mechanism, Appl. Phys. A 69 (1999), pp. 245–254.

(5) Y. Saito and S. Uemura, Field emission from carbon nanotubes and its application to electron sources, Carbon 38 (2000), pp. 169–182.

(6) H. Sugie, M. Tanemure, V. Filip, K. Iwata, K. Takahashi, and F. Okuyama, Carbon nanotubes as electron source in an X-ray tube, Appl. Phys. Lett. 78 (2001), pp. 2578–2580.

(7) S.C. Lim, K. Lee, I.H. Lee, and Y.H. Lee, Field emission and application of carbon nanotubes, Nano 2(2) (2007), pp. 69-89.

(8) P.R. Schwoebel, Field emission arrays for medical X-ray imaging, Appl. Phys. Lett. 88 (2006), 113902.

(9) G.Z. Yue, Q. Qiu, B. Gao, Y. Cheng, J. Zhang, H. Shimoda,
S. Chang, J.P. Lu, and O. Zhou, Generation of continuous and pulsed diagnostic imaging X-ray radiation using a carbon-nanotube-based field-emission cathode, Appl. Phys. Lett. 81(2) (2002), pp. 355–357.

(10) S. Wang, Z. Liu, S. Sultana, E. Schreiber, O. Zhou, and S. Chang, A novel high resolution micro-radiotherapy system for small animal irradiation for cancer research, Biofactors. 30(4) (2007), pp. 265–270.

(11) P. Yaghoobi and A. Nojeh, Electron emission from carbon nanotubes, Modern Phys. Lett. 21 (2007), pp. 1807–1830.

(12) R.V.N. Melnik and A. Povitsky, A special issue on modeling coupled and transport phenomena in nanotechnology, J. Comput. Theor. Nanosci. 3(4) (2006), pp. i-ii.

(13) R. Melnik, A. Povitsky, and D. Srivastava, Mathematical and computational models for transport and coupled processes in micro and nanotechnology, J. Nanosci. Nanotechnol. 8(7) (2008), pp. 3626–3627.

(14) A. Buldum and J.P. Liu, Electron field emission from carbon nanotubes: modeling and simulations, Mol. Simul. 30 (2004), pp. 199–203.

(15) N. Sinha, D. Roy Mahapatra, J.T.W. Yeow, R.V.N. Melnik, and D.A. Jaffray, Carbon nanotube thin film field emitting diode: understanding the system response based on multiphysics modelling, J. Comput. Theor. Nanosci. 4 (2007), pp. 1–15.

(16) N. Sinha, D. Roy Mahapatra, Y. Sun, J.T.W. Yeow, R.V.N. Melnik, and D.A. Jaffray, Electro-mechanical interactions in carbon nanotube based thin film field emitting diode, Nanotechnology 19 (2008), 025701.

(17) D. Roy Mahapatra, N. Sinha, J.T.W. Yeow, and R. Melnik, Field emission from strained carbon nanotube on cathode substrate, Appl. Surf. Sci. 255(5) (2008), pp. 1959–1966.

(18) R. Melnik and R. Mahapatra, Coupled effects in quantum dot nanostructures with nonlinear strain and bridging modelling scales, Comput. Struct. 85(11–14) (2007), pp. 698–711.
(19) N. Sinha, D. Roy Mahapatra, R.V.N. Melnik, and J.T.W. Yeow, Computational implementation of a new multiphysics model for field emission from CNT thin films, M. Babuk et al., eds., Lecture Notes in Computer Science, ICCS 2008, Part II, LNCS 5102, 2008, pp. 197–206.
(20) N. Sinha, D. Roy Mahapatra, J.T.W. Yeow, and R.V.N. Melnik, Multi-mode phonon controlled field emission from carbon nanotubes: device modeling and experiments, IEEE Proceedings of 7th International Conference on Nanotechnology, 2007, pp. 961–964.
(21) M. Wang, Z.H. Li, X.F. Shang, X.Q. Wang, and Y.B. Zu, Field enhancement array for carbon nanotube array, J. Appl. Phys. 98 (2005), 014315.
(22) G. Chen, D.H. Shin, T. Iwasaki, H. Kawarada, and C.J. Lee, Enhanced field emission properties of vertically aligned double-walled carbon nanotube arrays, Nanotechnology 19 (2008), 415703.
(23) D. Roy Mahapatra, N. Sinha, S.V. Anand, R. Krishnan, N.V. Vikram, R.V.N. Melnik, and J.T.W. Yeow, Design optimization of field emission from a stacked carbon nanotube array, NSTI-Nanotech 2008, Vol. 1, 2008, pp. 55–58, ISBN 978-1-4200-8503-7.
(24) Y. Peng, Y. Hu, and H. Wang, Fabrication of high-resolution multiwall carbon nanotube field emission cathodes at room temperature, J. Vac. Sci. Technol. 25 (2007), pp. 106-108.
(25) G.Y. Slepyan, S.A. Maksimenko, A. Lakhtakia, O. Yevtushenko, and A.V. Gusakov, Electrodynamics of carbon nanotubes: dynamic conductivity, impedance boundary conditions, and surface wave propagation, Phys. Rev. B 60(24) (1999), pp. 17136–17149.
(26) L. Wei and Y.N. Wang, Electromagnetic wave propagation in single-wall carbon nanotubes, Phys. Lett. A 333 (2004),
pp. 303–309.
(27) A. Svizhenko, M.P. Anantram, and T.R. Govindan, IEEE Trans Nanotech. 4 (2005), p. 557.
(28) R.H. Fowler and L. Nordheim, Proc. R. Soc. Lond. A 119 (1928), p. 173.
(29) Z.P. Huang, Y. Tu, D.L. Carnahan, and Z.F. Ren, Field emission of carbon nanotubes, in Encyclopedia of Nanoscience and Nanotechnology, H.S. Nalwa ed.,Vol. 3, 2004, pp. 401-416.
(30) D. Roy Mahapatra, S.V. Anand, N. Sinha and R.V.N. Melnik, High resolution surface imaging using a carbon nanotube array with pointed height distribution, NSTI-Nanotech 2009, Vol. 1, 2009, pp. 310–313, ISBN 978-1-4398-1782-7.
(31) D. Roy Mahapatra, N. Sinha, R.V.N. Melnik, and J.T.W. Yeow, Field emission properties of carbon nanotube arrays with defects and impurities, NSTI-Nanotech 2008, Vol. 3, 2008, pp. 729–732, ISBN 978-1-4200-8505-1.
(32) D. Roy Mahapatra, S.V. Anand, N. Sinha, R.V.N. Melnik, Enhancing field emission from a carbon nanotube array by lateral control of electrodynamic force field, Molecular Simulation, 35(6) (2009), pp. 512-519.